Dynamical behavior of a Brillouin fiber ring laser emitting two Stokes components

S. Randoux, V. Lecoeuche, B. Ségard, and J. Zemmouri
Laboratoire de Spectroscopie Hertzienne, Université des Sciences et Technologies de Lille, F-59655 Villeneuve d'Ascq CEDEX, France
(Received 16 November 1994)

The dynamics of a Brillouin fiber ring laser operating on the two first Stokes components is studied both theoretically and experimentally. The emergence of the second order Stokes wave is described within the framework of a coherent five-wave model that generalizes the usual three-wave model. The laser steady states are analytically characterized and the dynamics is numerically studied. The laser emission is stable except at high pumping rates for which the system exhibits periodic and quasiperiodic instabilities. Experimental results are in good agreement with the theoretical predictions.

PACS number(s): 42.65.Es, 42.50.Ne, 42.81.−i

I. INTRODUCTION

The dynamics of stimulated Brillouin scattering (SBS), which is one of the most dominant nonlinear effects in cw-pumped optical fibers, has recently captured considerable interest [1–3]. Resonantly coupling two electromagnetic waves and an acoustic wave through electrostriction, SBS can be a very low threshold phenomenon when the fiber is placed inside an optical resonator. Such a system is then called a SBS fiber laser [4] and it can exhibit various types of behaviors. Very stable single-mode cw regimes with linewidths as narrow as 30 Hz [5] have been obtained in high-finesse resonators [6] or in externally stabilized systems [7]. Mode-locked operation has been demonstrated with the aid of an intracavity acousto-optic modulator [8]. Finally, the observation of solitonic regimes has recently been achieved [9].

The first theoretical description of the Brillouin fiber ring laser dynamics was formulated by Bar-Joseph *et al.* [10]. In this model, the inertial response of the acoustic wave is neglected, the system dynamics being then described by equations for the pump and the SBS beam intensities. Such an instantaneous response model obviously fails when the characteristic evolution times of the system become comparable to the acoustic-wave relaxation rate. A more realistic description of the SBS ring laser dynamics is then given by the now well established three-wave SBS model [11]. This one takes into account the acoustic damping and correctly describes most of the experimentally observed regimes. Recently, for example, a Hopf bifurcation between steady and pulsed regimes has been evidenced in a Brillouin fiber ring laser [12].

However, at high enough pump power level, the first Stokes component, downshifted by $\mathcal{V}_s$ (the acoustic frequency) from the pump frequency, may generate a second Stokes component downshifted by $2\mathcal{V}_s$ from the pump frequency. Such a process can easily recur so that the second Stokes component may induce the appearance of a third-order Stokes line and so on. First evidenced in a Fabry-Pérot configuration [13], this "Stokes cascade" has also been pointed out in a Brillouin ring laser [11]. The description of this effect requires a generalization of the three-wave SBS model that only deals with two optical waves.

In Sec. II A of this paper, we develop a five-wave model that takes into account the appearance of the second-order Stokes wave. The resulting equations, completed by appropriate boundary conditions, then describe the dynamics of the first two Stokes components emitted by a SBS fiber ring laser. Section II B is devoted to a characterization of the system steady states; in particular, a threshold condition for the growth of the second-order Stokes wave is derived. The stability of the steady-state solutions is numerically investigated in Sec. III. Finally, in Sec. IV, experimental results are compared with the theoretical predictions. For the SBS laser studied, experiments and numerical simulations show that the steady "Brillouin mirror" regime is reached just above the first-order Stokes lasing threshold. The intensity of the first-order Stokes wave is then stable and increases with the input pump power up to the second-order Stokes lasing threshold. First of all, the appearance of this third optical wave does not destabilize the system but, at higher pumping levels, the interplay between the three optical waves results in the emergence of instabilities. Periodic oscillations at the frequency of the cavity free spectral range (FSR) are then observed. For higher input pump powers, new frequencies appear, giving rise to quasiperiodic regimes.

II. THEORETICAL DESCRIPTION

A. The five-wave model

In order to describe the time-dependent behavior of multiple SBS, let us first consider the propagation of a linearly polarized optical pump wave $\mathcal{E}_p(\omega_p,\mathbf{k}_p)$ in a single-mode fiber. $\mathbf{k}_p$ and ω_p are, respectively, the wave vector and the frequency of this forward-propagating wave, which can parametrically decay into a forward-propagating acoustic wave $\mathcal{M}_1(\omega_{a1},\mathbf{k}_{a1})$ and a backscattered Stokes wave $\mathcal{E}_{s1}(\omega_{s1},\mathbf{k}_{s1})$. The frequencies and the wave vectors of these waves are assumed to fulfill the resonance condition $\omega_{s1}=\omega_p-\omega_{a1}$ and the phase-matching relation $\mathbf{k}_p=\mathbf{k}_{a1}+\mathbf{k}_{s1}$. We now allow the first Stokes wave $\mathcal{E}_{s1}$ to be reduced to a backward-propagating acoustic wave $\mathcal{M}_2(\omega_{a2},\mathbf{k}_{a2})$ and a forward-propagating second-order Stokes component $\mathcal{E}_{s2}(\omega_{s2},\mathbf{k}_{s2})$. The resonance and

phase-matching conditions corresponding to this last interaction are then written, respectively, as $\omega_{s2}=\omega_{s1}-\omega_{a2}$ and $\mathbf{k}_{s1}=\mathbf{k}_{a2}+\mathbf{k}_{s2}$. Using the well justified plane-wave approximation and assuming a propagation along the z axis, the optical and acoustic waves can be written, respectively, as

$$\mathcal{E}_j=E_j(z,t)\exp i\{\omega_j t\pm k_j z\}+\text{c.c.}\ ,\quad j=p,s1,s2\ ,$$

$$\mathcal{M}_j=\rho_j(z,t)\exp i\{\omega_{aj}t\pm k_{aj}z\}+\text{c.c.}\ ,\quad j=1,2\ .$$

Substituting these expressions for $\mathcal{E}_p,\mathcal{E}_{s1},\mathcal{E}_{s2},\mathcal{M}_1,\mathcal{M}_2$ into the propagation equations of the optical and material waves [14] and using the slowly varying envelope approximation, we obtain the set of equations describing the five-wave interaction:

$$\begin{aligned}
&\frac{\partial E_p}{\partial t}+v\frac{\partial E_p}{\partial z}+\frac{\gamma}{2}E_p=iV_1\rho_1E_{s1}\ ,\\
&\frac{\partial E_{s1}}{\partial t}-v\frac{\partial E_{s1}}{\partial z}+\frac{\gamma}{2}E_{s1}=iV_1(\rho_1^*E_p+\rho_2E_{s2})\ ,\\
&\frac{\partial E_{s2}}{\partial t}+v\frac{\partial E_{s2}}{\partial z}+\frac{\gamma}{2}E_{s2}=iV_1\rho_2^*E_{s1}\ ,\\
&\frac{\partial \rho_1}{\partial t}+v_A\frac{\partial \rho_1}{\partial z}+\alpha_A\rho_1=iV_3E_pE_{s1}^*\ ,\\
&\frac{\partial \rho_2}{\partial t}-v_A\frac{\partial \rho_2}{\partial z}+\alpha_A\rho_2=iV_3E_{s1}E_{s2}^*\ ,
\end{aligned}\tag{1}$$

where v_A is the sound velocity and $v=c/n$ the light velocity in the fiber (refractive index: n). γ is the damping rate of the optical fields; it is linked to the absorption coefficient of the fiber α by the relation $\gamma=\alpha v$. $\alpha_A=\pi\Delta\nu_B$ is the damping coefficient of the acoustic waves, $\Delta\nu_B$ being the full width at half maximum of the spontaneous Brillouin gain curve. The optomaterial coupling constants are $V_1=(\pi n^2p_{12}c)/(\lambda_p\rho_0)$ and $V_3=(\pi n^5p_{12}\varepsilon_0)/(2\lambda_p v_A)$ where λ_p is the pump wavelength and ε_0 the free-space permittivity. Finally, p_{12} is the longitudinal elasto-optic coefficient in fused silica and ρ_0 the average fiber density.

The set of Eqs. (1) generalizes the usual three-wave SBS model by including a possible decay of the first-order Stokes wave into a second Stokes component and a backward-propagating acoustic wave. In order to describe Brillouin fiber ring lasers, these wave propagation equations have to be completed by the boundary conditions

$$\begin{aligned}
&E_p(z=0,t)=E_0\mu+RE_p(z=L,t)\ ,\\
&E_{s1}(z=L,t)=RE_{s1}(z=0,t)\ ,\\
&E_{s2}(z=0,t)=RE_{s2}(z=L,t)\ ,
\end{aligned}\tag{2}$$

where L is the fiber length. E_0 is the maximum pump-field amplitude coupled in the fiber and μ then plays the role of a dimensionless pump parameter. R is the amplitude feedback parameter. For the sake of simplicity, we will assume that it has the same value for the three optical waves and that it is real. Since it means that each optical wave is in exact resonance with one cavity mode, this last assumption is indeed very rough. However, it is commonly used [11,12] and supported by the good agreement between our theoretical and experimental results.

Following Ref. [15], the wave amplitudes can be rescaled with the new dimensionless variables:

$$\varepsilon_p=\frac{E_p}{E_0},\quad \varepsilon_{s1}=\frac{E_{s1}}{E_0},\quad \varepsilon_{s2}=\frac{E_{s2}}{E_0}\ ,$$

$$B_1=\frac{-i\rho_1\alpha_A}{|E_0|^2V_3},\quad B_2=\frac{-i\rho_2\alpha_A}{|E_0|^2V_3}\ .$$

The time can be written in units of cavity round-trip time and the spatial variable z in units of cavity length so that

$$\tau=\frac{vt}{L},\quad \zeta=\frac{z}{L}\ .$$

Since v_A/v is approximately equal to 10^{-5} in silica, the propagation of the acoustic wave can be neglected, and Eqs. (1) then become

$$\frac{\partial\varepsilon_p}{\partial\tau}+\frac{\partial\varepsilon_p}{\partial\zeta}+\frac{\beta}{2}\varepsilon_p=-gB_1\varepsilon_{s1}\ ,\tag{3a}$$

$$\frac{\partial\varepsilon_{s1}}{\partial\tau}-\frac{\partial\varepsilon_{s1}}{\partial\zeta}+\frac{\beta}{2}\varepsilon_{s1}=g(B_1^*\varepsilon_p-B_2\varepsilon_{s2})\ ,\tag{3b}$$

$$\frac{\partial\varepsilon_{s2}}{\partial\tau}+\frac{\partial\varepsilon_{s2}}{\partial\zeta}+\frac{\beta}{2}\varepsilon_{s2}=gB_2^*\varepsilon_{s1}\ ,\tag{3c}$$

$$\frac{1}{\beta_A}\frac{\partial B_1}{\partial\tau}+B_1=\varepsilon_p\varepsilon_{s1}^*+f(\zeta,\tau)\ ,\tag{3d}$$

$$\frac{1}{\beta_A}\frac{\partial B_2}{\partial\tau}+B_2=\varepsilon_{s1}\varepsilon_{s2}^*+f(\zeta,\tau)\ ,\tag{3e}$$

where

$$\beta=\frac{\alpha L}{v},\quad \beta_A=\alpha_A\frac{Lw}{v},\quad g=\frac{V_1V_3L|E_0|^2}{\alpha_Av}\ .$$

The boundary conditions, rephrased in a dimensionless form, are written as

$$\varepsilon_p(\zeta=0,\tau)=\mu+R\varepsilon_p(\zeta=1,\tau)\ ,\tag{4a}$$

$$\varepsilon_{s1}(\zeta=1,\tau)=R\varepsilon_{s1}(\zeta=0,\tau)\ ,\tag{4b}$$

$$\varepsilon_{s2}(\zeta=0,\tau)=R\varepsilon_{s2}(\zeta=1,\tau)\ .\tag{4c}$$

Equations (3) and (4), which are now our working equations, govern the dynamics of a Brillouin fiber ring laser able to operate on the first two Stokes components. Since the laser emission is initiated from noise, a Langevin noise source $f(\zeta,\tau)$ [16,17], which describes the thermal fluctuations of the medium, has been added to the right-hand side of Eqs. (3d) and (3e). Above the lasing threshold, this term is obviously much weaker than all the others and will therefore be neglected in the analytical calculation.

B. The laser steady states

The steady-state solutions without optical attenuation ($\beta=0$) are obtained by transforming the field complex

amplitudes to modulus-phase form and by dropping the time derivatives in Eqs. (4). All the field phases are then independent of ζ and the equations for the moduli are written as

$$\frac{dA_p}{d\zeta} = -gA_pA_{s1}^2 , \tag{5a}$$

$$\frac{dA_{s1}}{d\zeta} = -gA_{s1}A_p^2 + gA_{s1}A_{s2}^2 , \tag{5b}$$

$$\frac{dA_{s2}}{d\zeta} = gA_{s2}A_{s1}^2 , \tag{5c}$$

$$|B_1| = A_pA_{s1} , \tag{5d}$$

$$|B_2| = A_{s1}A_{s2} , \tag{5e}$$

where $A_p=|\varepsilon_p|$, $A_{s1}=|\varepsilon_{s1}|$, and $A_{s2}=|\varepsilon_{s2}|$. The stationary boundary conditions are written as

$$A_p(\zeta=0)=\mu+RA_p(\zeta=1) , \tag{6a}$$

$$A_{s1}(\zeta=1)=RA_{s1}(\zeta=0) , \tag{6b}$$

$$A_{s2}(\zeta=0)=RA_{s2}(\zeta=1) . \tag{6c}$$

Below the first-order Stokes lasing threshold, the amplitudes of the two Stokes waves are equal to zero and the pump-field amplitude then linearly increases with the control parameter: $A_p(\zeta)=A_p(0)=\mu/(1-R)$ (see Fig. 1).

Between the first- and second-order Stokes lasing thresholds, $A_{s2}(\zeta)=0$ and Eqs. (5a) and (5b) can be integrated [10,11] yielding the fixed-state longitudinal profiles of the pump and of the first-order Stokes wave [see Fig. 2(a)]:

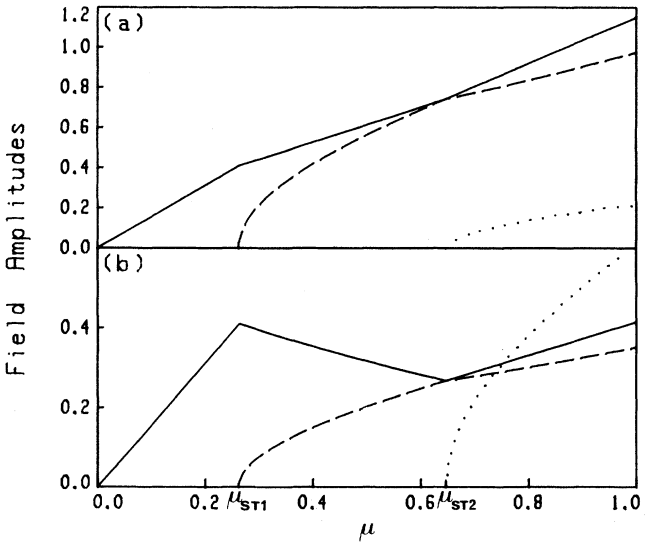

FIG. 1. Steady characteristics of the pump (solid line), first-order Stokes (dashed line), and second-order Stokes (dotted line) fields for $R=0.36$ and $g=6.04$. (a) At $\zeta=0$, (b) at $\zeta=1$. The numerical values of μ_{ST1} and μ_{ST2} are, respectively, 0.263 and 0.648.

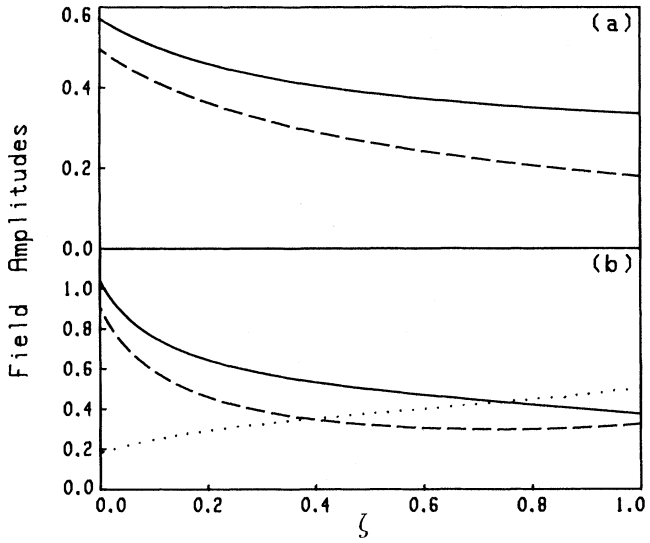

FIG.2. Fixed-state longitudinal profiles of the pump (solid line), first-order Stokes (dashed line), and second-order Stokes (dotted line) fields for $R=0.36$, $g=6.04$ and (a) $\mu=0.45$, (b) $\mu=0.90$.

$$A_p^2(\zeta)=\frac{\Omega(R^2-1)e^{-G\Omega}}{(R^2-1)e^{-G\Omega}-(R^2-e^{-G\Omega})e^{-G\Omega\zeta}} , \tag{7a}$$

$$A_{s1}^2(\zeta)=\frac{(R^2-e^{-G\Omega})\Omega e^{-G\Omega\zeta}}{(R^2-1)e^{-G\Omega}-(R^2-e^{-G\Omega})e^{-G\Omega\zeta}} , \tag{7b}$$

where $\Omega=A_p^2(0)-A_{s1}^2(0)=A_p^2(\zeta)-A_{s1}^2(\zeta)$ and $G=2g$. For a given value of $A_{s1}^2(0)$, $A_p^2(0)$ can be calculated by numerically solving the equation

$$R^2A_p^2(0)=[A_p^2(0)+(R^2-1)A_{s1}^2(0)] \times\exp[-G\{A_p^2(0)-A_{s1}^2(0)\}] .$$

The corresponding value of the control parameter μ, calculated by combining Eqs. (6a) and (7a), is

$$\mu=A_p(0)-R\left[\frac{\Omega(R^2-1)}{\exp(-G\Omega)-1}\right]^{1/2} .$$

It is then possible to plot the steady characteristics of the laser operating on the first-order Stokes line. As shown in Figs. 1(a) and 1(b), the increase in the first-order Stokes field amplitude does not have the same repercussion on the pump field characteristic at $\zeta=0$ and at $\zeta=1$. The pump depletion effect manifests through a diminution of the slope of this characteristic at $\zeta=0$ and through a slope sign change at $\zeta=1$. Putting $A_{s1}(0)=0$ in the two last equations simply leads to the analytical expression of the first-order Stokes lasing threshold:

$$\mu_{ST1}=\left[\frac{-\ln R}{g}\right]^{1/2}(1-R) .$$

The term $(1-R)$ expresses a diminution of the threshold value linked to the cavity effect on the pump field. If the recoupling of the pump wave is avoided, one then simply retrieves the result of Ref. [12]. Note, however, that expressions (7a) and (7b) remain valid if and only if $\Omega\neq 0$.

If $\Omega=0$, the resolution of Eq. (5b), associated with the limit condition of Eq. (6b), leads to

$$A_p^2(\zeta)=A_{s1}^2(\zeta)=\frac{1}{G\left[\zeta+\frac{R^2}{1-R^2}\right]} . \tag{8}$$

Nevertheless, this equalization of the two fixed-state longitudinal profiles can only be reached for a sufficiently high value of μ.

Above the second-order Stokes lasing threshold μ_{ST2}, the steady-state equations (5) have two invariants:

$$\theta=A_p^2(\zeta)-A_{s1}^2(\zeta)+A_{s2}^2(\zeta) , \tag{9a}$$

$$\Gamma=A_p^2(\zeta)A_{s2}^2(\zeta) . \tag{9b}$$

By combining Eqs. (6a), (6c), and (9b), we obtain

$$A_p(0)=\frac{\mu}{1-R^2} , \tag{10a}$$

$$A_p(1)=\frac{\mu R}{1-R^2} . \tag{10b}$$

This surprising result means that for $\mu>\mu_{ST2}$, the characteristic of the pump field no longer depends on the medium and is only determined by the cavity feedback parameter R. This characteristic is then a straight line and its slope is obviously lower than the one obtained in the passive regime for $\mu<\mu_{ST1}$ (Fig. 1). Appropriate combinations of Eqs. (6a), (6c), (9a), and (10a) allow one to express the constants θ and Γ as functions of μ and $A_{s2}^2(0)$:

$$\theta=\frac{1+R^2}{R^2}A_{s2}^2(0) ,$$

$$\Gamma=\frac{A_{s2}^2(0)\mu^2}{(1-R^2)^2} ,$$

and to establish that $\Gamma-\theta^2/4>0$ whatever the values of $A_{s2}^2(0)$, μ, and R may be. Taking into account the boundary condition (6c), Eqs. (5) can be analytically integrated, yielding

$$A_{s2}^2(\zeta)=\frac{\theta}{2}+\sqrt{D}\tan\left[G\sqrt{D}(\zeta-1)+\arctan\left[\frac{[A_{s2}^2(0)]/R^2-(\theta/2)}{\sqrt{D}}\right]\right] , \tag{11}$$

where $D=\Gamma-\theta^2/4$. The stationary longitudinal profiles $A_{s1}^2(\zeta)$ and $A_p^2(\zeta)$ are then easily deduced from Eqs. (9a), (9b), and (11) [see Fig. 2(b)]. The steady characteristics of the two Stokes fields are obtained numerically: for a given value of $A_{s2}^2(0)$, μ is computed by solving Eq. (11) in which one imposes $\zeta=0$. Figure 1(a) shows that the appearance of the second-order Stokes wave entails a diminution of the slope of the first-order Stokes field characteristic at $\zeta=0$. By considering $A_{s2}^2(\zeta)$ as a first-order perturbative term in Eqs. (5), it is possible to establish that $A_p^2(\zeta)=A_{s1}^2(\zeta)$ for $\mu=\mu_{ST2}$. This result is illustrated in Figs. 1(a) and 1(b), which show that the intersection of the pump and of the first-order Stokes field characteristics coincides with the second-order Stokes lasing threshold. At this point, the longitudinal field profiles are given by Eq. (8). Furthermore, this equation, associated with Eq. (10), yields the analytical expression of μ_{ST2}:

$$\mu_{ST2}=\frac{1}{R}\left[\frac{(1-R^2)^3}{G}\right]^{1/2} .$$

The laser steady states being now well characterized, their stability can be theoretically studied by linearizing Eqs. (4) around the stationary solution. However, this procedure leads to differential equations that are complicated and difficult to solve analytically; we will then restrict ourselves to the numerical study presented in the next section.

III. FIVE-WAVE DYNAMICS: NUMERICAL STUDY

In order to solve numerically Eqs. (3) in the presence of boundary conditions (4), we used an algorithm based on the method of characteristics. In the results that we illustrate in this section, the physical data used to compute the reduced parameters are chosen in order to describe the experimental system depicted in Sec. IV. At the working wavelength of 800 nm, $\Delta\nu_B$ is estimated to be 60 MHz [18]. p_{12}, v_A, and ρ_0 are, respectively, equal to 0.286, 5.96×10^3 m s^{-1}, 2.21×10^3 kg m^{-3} [11]. The active medium is a single-mode fiber of length $L=12$ m with a 2.75-μm core diameter ($n=1.45$); its absorption coefficient α is 1.2×10^{-3} m^{-1}. The maximum power launched in the fiber is 130 mW and E_0 is then equal to 3.37 MV/m. The parameter values deduced from these physical data and used for numerical simulations are then $g=6.04$, $\beta_A=10.93$, $\beta=0.01$. Finally, the feedback parameter that we used to describe our Brillouin fiber ring laser is $R=0.36$.

The laser dynamics can be synthesized in the single numerical bifurcation diagram presented in Fig. 3. It is obtained by numerically solving Eqs. (3) and (4) for a given μ and for long enough time to ensure that the system evolution is well after the transient process. Then we plot the maximum values reached by $A_{s1}(\zeta=0,\tau)$ inside a final time interval that is much greater than the system characteristic time (that is, the cavity round-trip time T_r). Finally, starting from initial conditions characterizing the system state at the end of the integration, the process is repeated for a greater value of μ. The dashed line in Fig. 3 represents the analytically calculated stationary state for $\beta=0$. Above the first-order Stokes lasing threshold, the computed points of the bifurcation diagram nearly coincide with the steady characteristic, the difference coming from the optical attenuation. The stability of the system, already discussed in Ref. [19], is then related to the monomode character of the first-order Stokes laser emission in short enough cavities. As shown in Fig. 3, this stability persists up to and well above the second-order Stokes lasing threshold. However, when μ becomes greater than μ_c, the system abruptly destabilizes and periodic instability regimes are then reached. Further in-

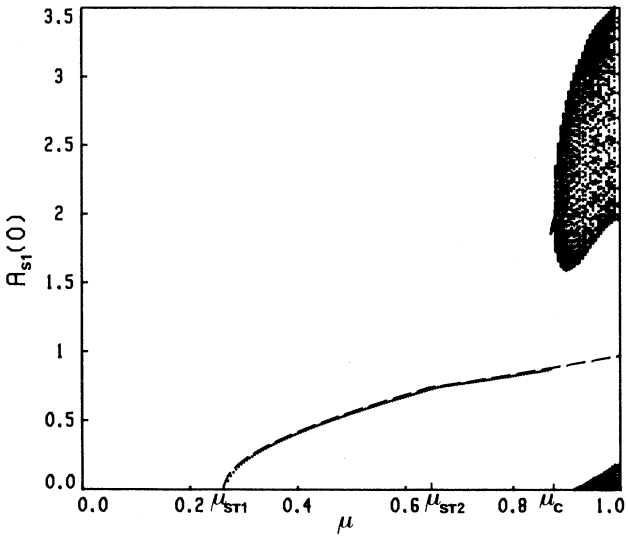

FIG. 3. Numerically computed bifurcation diagram of the Brillouin fiber ring laser. The dashed line represents the analytically calculated system steady state and the numerical value of μ_c is 0.870.

crease in the value of μ leads to the emergence of quasiperiodic instability regimes. Let us point out here that the destabilization scenario thus described for $A_{s1}(\zeta=0, \tau)$ is identical for the dynamical variables $A_p(\zeta=0,\tau)$ and $A_{s2}(\zeta=0,\tau)$. As illustrated in Figs. 4(a) and 4(b), the periodic instabilities are characterized by a frequency

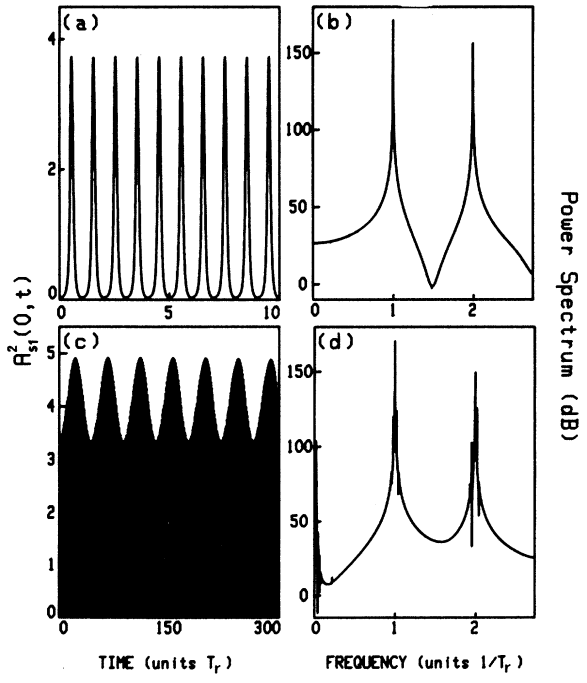

FIG. 4. Temporal evolution of the first-order Stokes wave intensity and associated power spectrum for (a),(b) periodic state ($\mu=0.875$); (c),(d) quasiperiodic state ($\mu=0.882$).

equal to the cavity FSR. Quasiperiodicity manifests itself through the appearance of a low-frequency envelope that modulates the signal oscillating at the cavity FSR frequency [Fig. 4(c)]. The spectral analysis reveals a multipeak structure that superimposes itself on the spectrum of the periodic signal [Fig. 4(d)].

Let us now describe more precisely the nature of the bifurcation occurring between the stationary and the periodic state at $\mu=\mu_c$. As already mentioned, the system destabilization is abrupt; this suggests that one should sweep μ back and forth around μ_c. This sweeping was performed with the method used to compute the bifurcation diagram of Fig. 3 and the result is presented in Fig. 5. By increasing μ, the stationary solution becomes unstable for $\mu>\mu_c$ and the system precipitates towards another attractor, that is, a limit cycle. The backward sweep shows that the switch from the limit cycle to the steady state occurs for $\mu=\mu_s$. Since $\mu_s<\mu_c$, a range of values of μ for which generalized bistability between a limit cycle and the stationary solution exists. The bifurcation associated with the coexistence of these two attractors is then a subcritical Hopf bifurcation [20]. Note that the width of the hysteresis is small and the generalized bistability effect could then be difficult to evidence experimentally. Another way to characterize the nature of the bifurcation consists of continuously sweeping the control parameter at a very slow rate. As shown in Fig. 6, the discontinuous jump from the steady state to the limit cycle is then expressed through an explosive growth of the oscillation amplitude. Even if it generates dynamical effects on the position of the bifurcation points, this last sweeping method provides a global description of the laser dynamics. Moreover, as it is easy to implement experimentally, we will use it in Sec. IV.

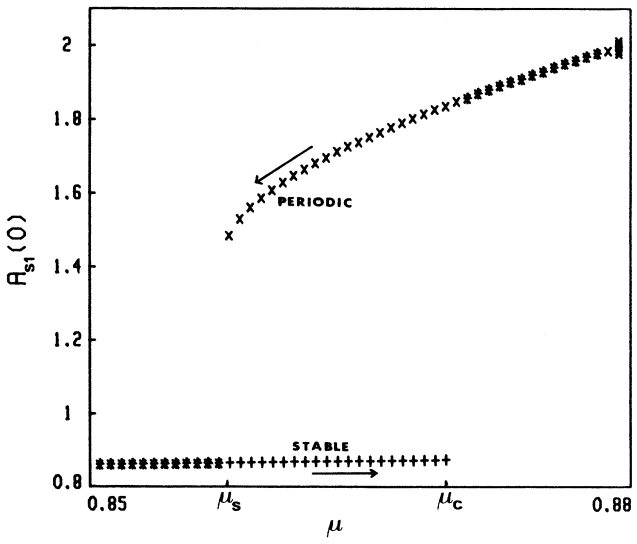

FIG. 5. Numerical bifurcation diagram illustrating the coexistence between the stationary solution and a limit cycle. + indicates the system state as the control parameter increases. × corresponds to the system state as μ decreases. The numerical value of μ_S is 0.857.

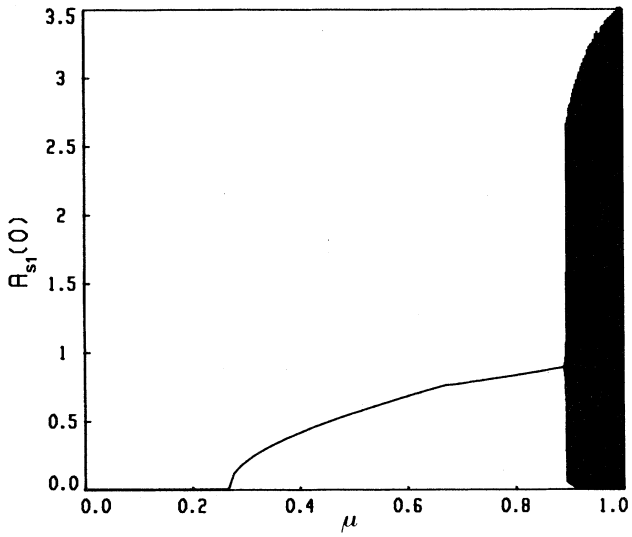

FIG. 6. Evolution of the amplitude of the first-order Stokes field as the control parameter μ is slowly increased.

When the system evolves on the limit cycle, interesting information concerning the energy exchanges between optical waves can be obtained by considering the field longitudinal profiles inside the fiber at different times. As shown in Fig. 7, the instability regimes are characterized by the propagation and by the interactions of Stokes

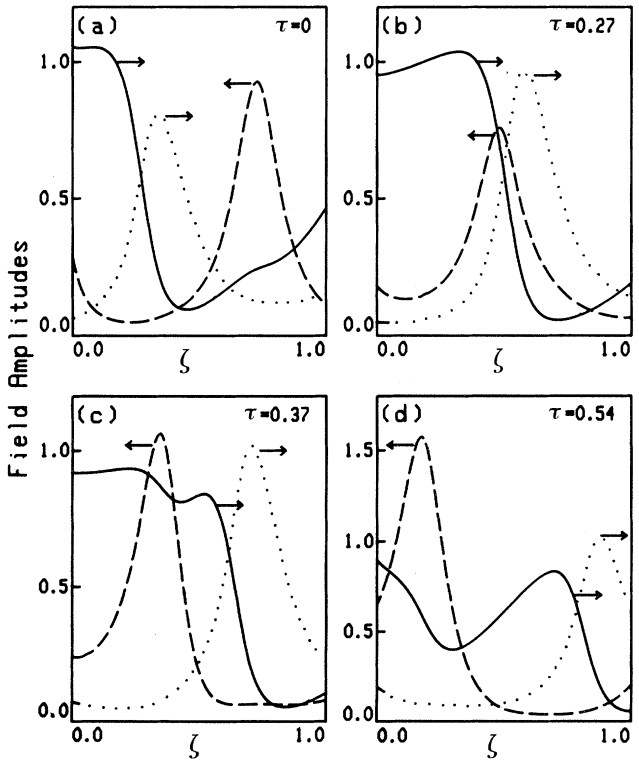

FIG. 7. Longitudinal profiles of the fields along the fiber axis at different times: pump (solid line), first-order Stokes (dashed line), and second-order Stokes (dotted line). The system evolves on the limit cycle (μ=0.876).

pulses along the optical fiber. In order to understand the nature of these interactions, let us consider initial conditions such that a first-order Stokes pulse is localized near ζ=1 [Fig. 7(a)]. This backward-propagating pulse encounters a forward-propagating second-order Stokes pulse and is depleted [Fig. 7(b)]. The forward-propagating pulse then exhibits noticeable gain and pursues its propagation toward the output end of the fiber. During this time, the first-order Stokes pulse encounters a fresh pump envelope which is then strongly depleted while the pulse amplitude grows [Figs. 7(c) and 7(d)]. Finally, because of the cavity effect, the amplitudes of the two Stokes pulses are multiplied by R and the process starts again. However, the periodic motion thus described rapidly disappears if μ increases (Fig. 3). During the interaction between the two Stokes waves, the first-order Stokes pulse is depleted and the trailing edge of the second-order Stokes pulse is then less amplified than the leading edge [Figs. 7(a) and 7(b)]. For high enough pumping rates, the depletion can be so important that the "center of mass" of the second-order Stokes pulse is slightly shifted in the forward direction. A similar process occurs during the interaction between the pump and the first-order Stokes waves [9]: the leading edge of the first-order Stokes pulse is more amplified than the trailing edge, which interacts with an already depleted pump wave [Fig. 7(d)]. The center of mass of the first-order Stokes pulse is then shifted in the backward direction. So, from one cavity round trip to the other, the two Stokes pulses collide at different positions in the optical fiber and then experience a slightly different gain. This effect is thus responsible or the emergence of the quasi-periodic instability regimes.

IV. EXPERIMENTS

The experimental setup used for the generation of multiple SBS in a ring cavity is schematically shown in Fig. 8. The pump source consists of a single-mode titanium-sapphire laser (Coherent 899-29), pumped by an argon ion laser (Coherent Innova 400), and operating at 800 nm. The titanium-sapphire laser, characterized by a 500-kHz linewidth, is optically isolated from the Brillouin ring laser by a Faraday isolator. An acousto-optic

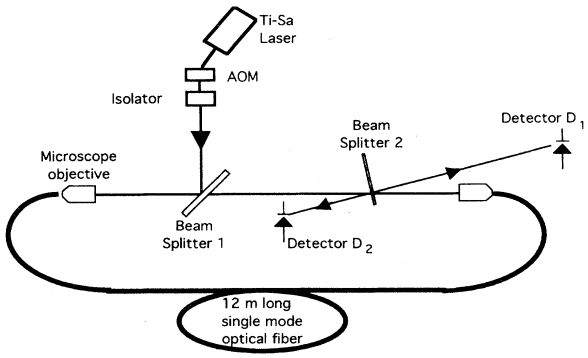

FIG. 8. Experimental setup. The reflectivity of beamsplitters 1 and 2 are, respectively, equal to 0.3 and 0.04.

modulator (AOM) allows one to control the incident pump power. The polarization-preserving fiber is cabled in order to limit external perturbations and has a cutoff wavelength of 630 nm for monomode propagation. Two 20× microscope objectives are used to couple the light into and out of the optical fiber. The feedback is simply achieved by reinjecting the output beam at the entrance end of the fiber. In this ring configuration, each optical wave propagates in a single direction and the counterpropagative beams can be spatially separated by inserting a low reflectivity beam splitter into the cavity. The forward-propagating (pump+even Stokes components) and backward-propagating (odd Stokes components) beam powers are then respectively detected by the silicium photodiodes D_1 and D_2. These have a rise time of 5 ns and are connected to a digital oscilloscope (Lecroy 9400), which has a data sampling rate of 10 ns. Finally, an external Fabry-Pérot interferometer (not displayed in Fig. 8) was used to monitor the emergence of the different Stokes components.

In Sec. III, we have mentioned that the feedback parameter used to describe our SBS fiber ring laser is equal to 0.36. In fact, this value is approximate and results from an estimation of the resonator round-trip losses. Moreover, it drifts slightly because of unavoidable environmental fluctuations and any quantitative experimental verification of the theoretical results (e.g., the threshold values) is then delicate. Nevertheless, a qualitative comparison between the theoretical and experimental results shows that our model incorporates all the essential ingredients characterizing the laser dynamics.

An overview of the system dynamics can be obtained by slowly sweeping the input pump power with the aid of the AOM. The signal recorded by the photodiode D_1 during this sweeping is presented in Fig. 9(a). Since the frequency shift between the pump and the second-order Stokes waves is several tens of GHz [18], this signal is directly proportional to the sum of the two field powers, that is, $A_p^2(\zeta=1)+A_{s2}^2(\zeta=1)$. The signal recorded at the same time by photodiode D_2 is shown in Fig. 9(b). It is proportional to the power of the first-order Stokes wave, that is, $A_{s1}^2(\zeta=0)$. A direct comparison between Figs. 6 and 9(b) is then possible and one can note a good qualitative agreement between the experimental and the numerically predicted behaviors. In particular, the explosive growth of the instability amplitude that we observe experimentally confirms the existence of a subcritical Hopf bifurcation between the stationary and the time-dependent states. For input pump powers lower than the second-order Stokes lasing threshold, the signal presented in Fig. 9(a) can be directly compared to the pump-field characteristic of Fig. 1(b). Above this threshold, the two forward-propagating waves are detected and the observed instabilities are then linked to the oscillation of the two associated dynamical variables.

The temporal analysis of the instabilities observed in the first-order Stokes emission (photodiode D_2) was performed at constant input pump powers. Some examples of periodic and quasiperiodic signals and of their associated power spectrum are presented in Fig. 10. As evidenced in Figs. 10(a) and 10(b), the periodic instabilities are characterized by a frequency equal to the cavity FSR: 16.9 MHz. By increasing the input pump power, quasiperiodic instability regimes of Fig. 10(c) are observed. As

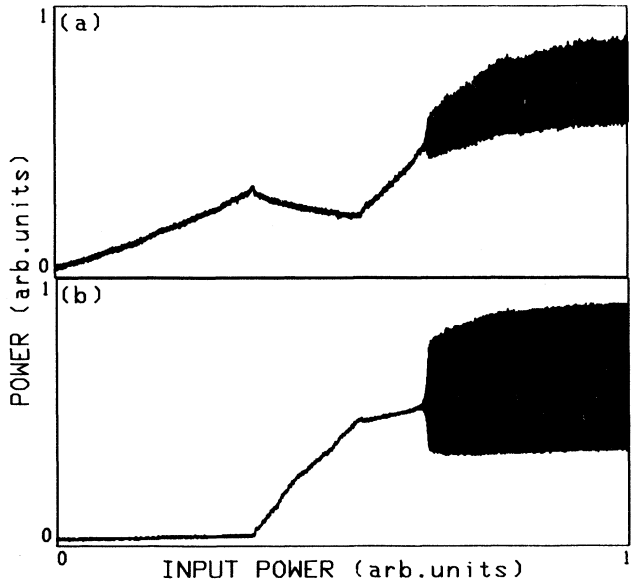

FIG. 9. (a) Power detected (photodiode D_1) in the forward direction, (b) power detected (photodiode D_2) in the backward direction, while slowly sweeping the input pump power.

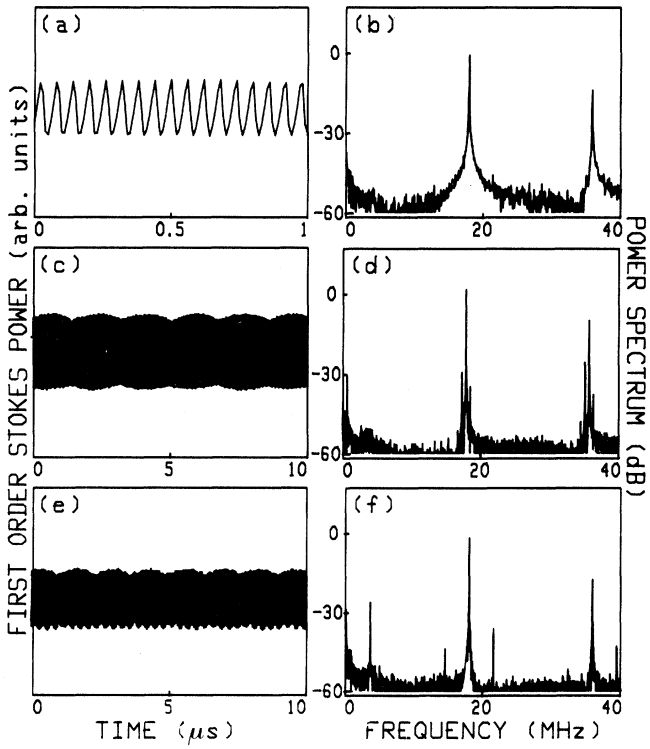

FIG. 10. Temporal evolution of the first-order Stokes power and associated power spectrum: (a),(b) periodic instabilities at the FSR frequency; (c),(d) and (e),(f) quasiperiodic instabilities.

shown in Fig. 10(d) the corresponding power spectrum becomes richer with a low frequency of about 600 kHz. In other experimental conditions characterized by a higher coupled power and by a lower feedback efficiency, this low frequency value drastically changes and becomes about 3.3 MHz [Figs. 10(e) and 10(f)]. This result, not mentioned in Sec. III, is, however, well confirmed by numerical computations performed with other sets of parameters.

V. CONCLUSION

The dynamics of a Brillouin fiber ring laser emitting two Stokes components was studied both experimentally and theoretically. At first, a theoretical model involving three optical and two acoustic waves was elaborated on in order to include a possible decay of the first Stokes component into a second-order Stokes wave. Taking into account the boundary conditions characterizing the ring laser, the system steady states were studied, yielding analytical expressions for the two Stokes lasing thresholds. A numerical study of the stability of these steady states was performed with parameters characterizing the experimental conditions. It was then demonstrated that the system destabilizes, via a subcritical Hopf bifurcation, towards periodic and quasiperiodic instability regimes. All these predictions are in good agreement with our experimental results.

Although no chaotic behavior was observed in experiments, numerical simulations evidence a transition from quasiperiodicity to chaos for values of the pump parameter larger than those actually available in the experiments. However, one can conjecture that such pumping rates would be sufficiently high to induce the emergence of a third Stokes component, which should noticeably influence the system dynamics. This last effect is obviously not taken into account in our model. Let us emphasize that, for parameters different from those describing our experiments, the simulations show other destabilization scenarios such as sequences of period doubling which always appear at high pumping levels. Obviously, these numerical predictions require an experimental corroboration. Improvement of the experimental setup is in progress to provide access to these possible domains of chaos. Moreover, a theoretical model, involving a third Stokes component, is equally studied in order to check its effect on the laser dynamics.

Another nonlinear effect prone to influencing the system dynamics is the optical Kerr effect. By taking it into account, the phase dynamics then plays a nontrivial role and the nonlinear refraction can be responsible for self-phase and self-amplitude modulation [11]. However, it remains a perturbative effect and its study, although numerically possible, is difficult to realize from an experimental point of view. Finally, an important parameter is the length of the optical fiber. By increasing it, one decreases the cavity FSR and then favors longitudinal mode competition [19]. The first-order Stokes emission can then become unstable for a given range of input pump power values. Thus, the previously described scenario of the Stokes cascade could be altered.

ACKNOWLEDGMENTS

The authors wish to thank J. C. Garreau for a careful reading of the manuscript. The Laboratoire de Spectroscopie Hertzienne is Unité associé au CNRS.

[1] M. Dämmig, G. Zinner, F. Mitschke, and H. Welling, Phys. Rev. A **48**, 3301 (1993).
[2] R. G. Harrison, J. S. Uppal, A. Johnstone, and J. V. Moloney, Phys. Rev. Lett. **65**, 167 (1990).
[3] C. C. Chow and A. Bers, Phys. Rev. A **47**, 5144 (1993).
[4] K. O. Hill, B. S. Kawasaki, and D. C. Johnson, Appl. Phys. Lett. **28**, 608 (1976).
[5] S. P. Smith, F. Zarinetchi, and S. Ezekiel, Opt. Lett. **16**, 393 (1991).
[6] L. F. Stokes, M. Chodorow, and H. J. Shaw, Opt. Lett. **7**, 509 (1982).
[7] D. R. Ponikvar, and S. Ezekiel, Opt. Lett. **6**, 398 (1981).
[8] B. S. Kawasaki, D. C. Johnson, Y. Fujii, and K. O. Hill, Appl. Phys. Lett. **32**, 429 (1978).
[9] E. Picholle, C. Montes, C. Leycuras, O. Legrand, and J. Botineau, Phys. Rev. Lett. **66**, 1454 (1991).
[10] I. Bar-Joseph, A. A. Friesem, E. Lichtman, and R. G. Waarts, J. Opt. Soc. Am. B **2**, 1606 (1985).
[11] J. Botineau, C. Leycuras, C. Montes, and E. Picholle, J. Opt. Soc. Am. B **6**, 300 (1989).
[12] C. Montes, A. Mamhoud, and E. Picholle, Phys. Rev. A **49**, 1344 (1994).
[13] K. O. Hill, D. C. Johnson, and B. S. Kawasaki, Appl. Phys. Lett. **29**, 185 (1976).
[14] Y. R. Shen and N. Bloembergen, Phys. Rev. **6**, A1787 (1965).
[15] W. Lu, A. Johnstone, and R. G. Harrison, Phys. Rev. A **46**, 4114 (1992).
[16] R. W. Boyd, K. Rzazewski, and P. Narum, Phys. Rev. A **42**, 5514 (1990).
[17] A. L. Gaeta and R. W. Boyd, Phys. Rev. A **44**, 3205 (1991).
[18] G. P. Agrawal, *Nonlinear Fiber Optics* (Academic, New York, 1989).
[19] S. Randoux, V. Lecoeuche, B. Ségard,and J. Zemmouri, Phys. Rev. A **51**, 4345 (1995).
[20] J. M. T. Thompson, H. B. Stewart, and Y. Ueda, Phys. Rev. E **49**, 1019 (1994).